ELSEVIER

Catalysis Today 41 (1998) 261–275

CATALYSIS TODAY

Characterisation of heterogeneous catalysts by EXAFS

G. Vlaic[a,b,*], D. Andreatta[a], P.E. Colavita[a]

[a]*Dipartimento di Scienze Chimiche, Università di Trieste, Via L. Giorgeri 1, 34127 Trieste, Italy*
[b]*Sincrotrone Trieste SCpA, S.S.14, km 163.5, 34012 Trieste, Italy*

Abstract

EXAFS spectroscopy extracts structural information from a sample analysing its X-ray absorption spectrum. It allows us to determine the chemical environment of an element, in any aggregation state and under any kind of atmosphere, in terms of number and type of neighbours, interatomic distances and structural disorder. This determination is confined within a 4–8 Å radius from the element and does not include immediate stereochemical information.

These characteristics look like disadvantages, but they are virtues instead. In fact EXAFS does not require long-range ordered structures, so it becomes a powerful structural local probe.

We present in this paper a brief phenomenological explanation of the EXAFS signal and a short description of data collection and data analysis methodologies. Moreover, we report two examples which show how EXAFS can be successfully applied in catalysis.

Keywords: EXAFS; Spectroscopy; Structure of catalysts

1. Introduction

EXAFS spectroscopy extracts structural information from a sample analysing its X-ray absorption spectrum. It allows us to determine the chemical environment of an element – in any aggregation state and under any kind of atmosphere – in terms of number and type of neighbours, interatomic distances and structural disorder. This determination is confined within a 4–8 Å radius from the element and does not include immediate stereochemical information.

These characteristics look like disadvantages, as EXAFS is compared to other X-ray techniques like those based on diffraction phenomena, but they are its virtues instead. Besides allowing in situ studies, EXAFS does not require long-range ordered structures, so it becomes a powerful structural local probe.

EXAFS spectroscopy is an important technique in several fields of natural science, from physics to biochemistry. Particularly, in catalysis, since samples show highly disordered structures and since no restrictions exist on physical state or sample environment, EXAFS is one of the few tools for structural investigation [1].

In the following sections, theoretical bases underlying EXAFS and data analysis methods are illustrated briefly. At last, two examples of the role that EXAFS can play in catalysis are showed.

2. Origin of the EXAFS signal

The X-ray linear absorption coefficient for an atom, which is indicated by μx, is a monotone decreasing function of energy. It shows some discontinuities known as absorption edges [2]. They occur when

*Corresponding author.

0920-5861/98/$32.00
PII S0920-5861(98)00055-8

the energy of the incident photons is equal to the binding energy of a particular electron of the atom. Fig. 1 shows this behaviour for Rh atoms. It is possible to recognise four edges due to K and L electrons.

The edge energy is characteristic of each atom, so the absorption spectrum of a sample shows many edges that match threshold energies of the elements contained in it.

The absorption coefficient decreases monotonously between two edges with energy only in the case of isolated atoms (monoatomic gas). In any other situation the spectrum shows oscillations that extend from the edge to some hundreds of eV. Fig. 5 shows the absorption spectrum for metallic Rh at K edge.

When the incident photon has a greater energy than the edge energy, it is able to extract a core electron. The photoelectron emitted in this process has a kinetic energy equal to: $E=E_x-E_0$.

The photoelectron can be represented as a wave with wave vector modulus:

$$|\mathbf{k}| = \frac{2\pi}{\lambda} = \sqrt{\frac{8\pi^2 m(E_x - E_0)}{h^2}} = \sqrt{0.2624 \cdot E}.$$

In the case of an isolated atom, the photoelectron propagates as a non-perturbed isotropic wave (Fig. 2(a)). In the presence of neighbours a scattering process can take place instead (Fig. 2(b)). This leads to an interference phenomenon involving original and scattered waves that modify the interaction probability between electrons and incident photons. Constructive interference increases while destructive interference decreases the absorption coefficient of an emitting atom.

The EXAFS oscillation is strictly related to the interference phenomenon. The total scattering amplitude depends on type and number of neighbours. The type of interference, for a given energy of the photoelectron, depends on the distance between emitting and scattering atoms and their nature, so the EXAFS signal contains information on interatomic distances too.

It is theoretically proved that the EXAFS signal given by only one type of scatterers at a single distance is a sinusoidal oscillation. In the presence of several atom types and/or distances the signal appears more complicated, nevertheless it is the sum of various sinusoidal functions. The EXAFS signal also contains information on thermal and structural disorder.

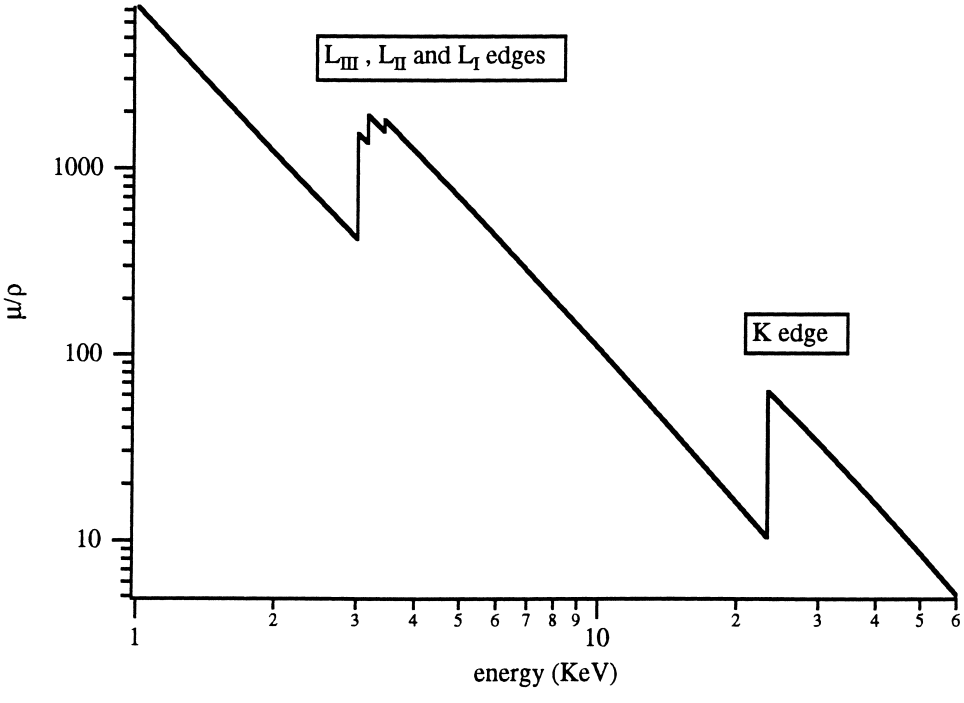

Fig. 1. Absorption spectrum of atomic Rh.

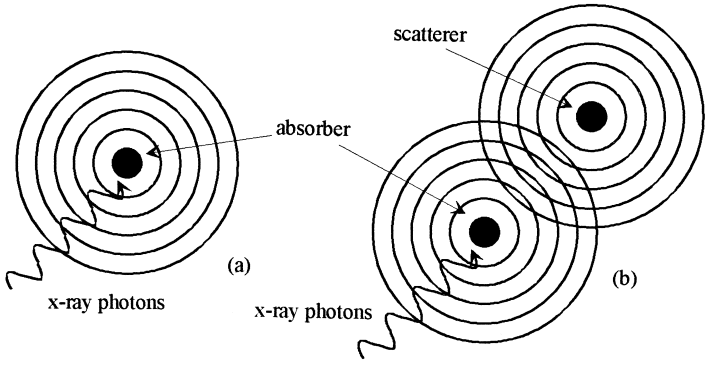

Fig. 2. Scattering processes.

The EXAFS signal $\chi(k)$ is usually defined as a function of wave vector **k** [3]. It is mathematically defined as follows:

$$\chi(k) = \frac{\mu x - \mu_1 x}{\mu_1 x} = \frac{\mu x}{\mu_1 x} - 1,$$

where μx is the experimental absorption coefficient and $\mu_1 x$ is the intrinsic atomic absorption coefficient. The aim of dividing by $\mu_1 x$ is the normalisation of the signal.

For core electrons, within the dipole approximation, the probability of X-ray absorption is given by

$$P_{\mathrm{if}} = \frac{2\pi^2 e^2}{m^2 \omega} |M_{\mathrm{if}}|^2 \rho(E_{\mathrm{f}}),$$

where i and f stand for the initial and final states of the electron, e and m are its charge and mass, $\rho(E_{\mathrm{f}})$ is the state density available to the electron (it is considered as a free electron so there is a continuous distribution of states), ω is the incident photon frequency and $|M_{\mathrm{if}}|$ is a dipole matrix element related to the transition of the electron from i to f state.

$$|M_{\mathrm{if}}| = \langle \psi_{\mathrm{f}} | \mathbf{p} \cdot \mathbf{e} | \psi_{\mathrm{i}} \rangle,$$

where **p** is the momentum operator, **e** is the electric field vector of the X photon, ψ_{f} and ψ_{i} are wave functions for i and f states.

ψ_{f} depends on the absorbed photon energy and can be written as a linear combination of two terms: the wave function for the photoelectron outgoing the excited atom and a perturbing term ψ_{sc} taking account for back-scattering.

Absorption coefficient is proportional to absorption probability, so

$$\chi(k) = \frac{\langle \Psi_{\mathrm{out}} + \Psi_{\mathrm{sc}} | \mathbf{p} \cdot \mathbf{e} | \Psi_{\mathrm{i}} \rangle}{\langle \Psi_{\mathrm{out}} | \mathbf{p} \cdot \mathbf{e} | \Psi_{\mathrm{i}} \rangle} - 1.$$

In 1974 Stern [4] suggested the following mathematical expression for the EXAFS signal:

$$\chi(k) = \frac{1}{k} \sum_i \frac{N_i}{R_i^2} \exp(-2\sigma_i^2 k^2) \times \exp\left(\frac{-2R_i}{\lambda(k)}\right) |f_i(k)| \sin[2kR_i + \Phi_i(k)],$$

where k is the wave vector modulus for the photoelectron, N_i is the number of atoms of type i at distance R_i from the absorber, the exponential term $\exp(-2\sigma_i^2 k^2)$ takes account of fluctuations on distances due to structural and/or thermal disorder, the exponential term $\exp(-2R_i/\lambda(k))$ takes account of finite elastic mean free paths of photoelectrons $\lambda(k)$ (between 5 and 10 Å for photoelectron energies from 30 to 1000 eV), $|f_i(k)|$ is the scattering amplitude function characteristic of the first atom and $\Phi_i(k)$is a phase function which takes account of the varying potential field along which the photoelectron moves, also it can be expressed as the sum of two potential terms, $\Phi_i(k) = 2\delta(k) + \varphi_i(k)$, the former given by the absorber, and the latter given by the scatterer.

This EXAFS equation is valid in the case of non-oriented samples (crystalline powders, solutions and gases) and also for monocrystals, whenever a common X-ray tube is used. Using synchrotron light sources

with monocrystals implies a correction of the equation: it must be multiplied by $3\cos^2\theta$, where θ is the angle between the absorber–scatterer axis and the synchrotron orbital plane. This term takes account of polarisation of synchrotron light (electric field vector lies on the orbital plane).

This formula is based on two hypotheses:

1. only single back-scattering processes occur, excluding multiple scattering processes, which are important only for low k values (when the mean free path of the electron is long, about 10–100 Å for energies between 0 to 20 eV) and for collinear or nearly collinear systems at every energy;
2. thermal or static disorder is moderate and distance distributions can be described with Gaussian distributions.

In this way it is possible, knowing phase and amplitude functions, to obtain structural information about the sample by the EXAFS signal analysis.

3. Experimental methods

The most common EXAFS beam-line works in transmission. It collects data measuring how beam intensity decreases as it passes through the sample while scanning energy.

As in any spectroscopy a light source is needed. EXAFS spectroscopy requires a polychromatic X-ray source as the bremsstrahlung of an X-ray tube or the synchrotron light of a storage ring. The former was the first source used for spectra recording but it gives a low quality signal that takes long recording time because of bremsstrahlung low intensity. Due to this, EXAFS spectroscopy remained only a scientific curiosity until the utilisation of synchrotron light which has been up to now the best light source to perform EXAFS measurements. Fig. 3 shows a sketch of a typical EXAFS beam-line working in transmission.

The monochromator allows to obtain photons with fixed energies or to make an energy scanning. Experimental spectra are recorded scanning energy from about 100 eV below the edge to 1000 eV above it. Energy steps are of 2 or 3 eV and each point takes 1 or 2 s.

As it is well known, Lambert–Beer law relates intensities I_0 and I to the absorption coefficient:

$$\ln\frac{I_0}{I} = \mu x.$$

Owing to the angular rotation of the crystals inside the monochromator, the beam can shift up or down. Light must pass through the sample always at the same position, so either the sample follows the beam by placing it on a micrometric table, or it is necessary to change the monochromator mechanism to obtain a fixed beam.

There is also a different experimental set-up useful at collecting data from diluted samples: it measures the fluorescent photons emitted by absorbing atoms [5].

A spectrum recording takes from 15 min up to 3 h, so it is impossible to perform kinetic studies and only in-equilibrium systems can be analysed. However, there are two other EXAFS techniques which take shorter recording times. The former is known as "Quick-EXAFS" [6] and requires only a couple of minutes. The latter is dispersive EXAFS [7] and takes a couple of seconds.

4. Data analysis

Nowadays there is no standard method for data analysis, but there is an International Committee that

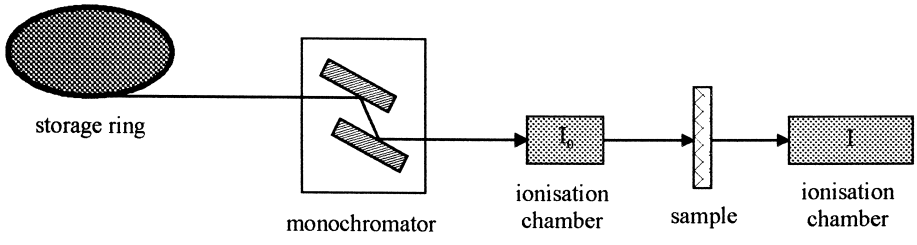

Fig. 3. Schematic EXAFS beam-line.

is trying to establish standard procedures. Until now it gave only recommendations contained in two reports [8,9]. Owing to this and to the large number of particular cases, a long training period is needed to obtain correct information.

Programs used for carrying out data analysis in the following examples were written by Michalowlcz [10] taking care of the recommendation mentioned above; this package uses Fourier transform techniques. More advanced programs perform the analysis directly on raw data [11].

First step in data analysis is signal extraction by background removing. This delicate operation can be divided into three steps:

1. choosing threshold energy, for wave vector definition;
2. pre-edge extrapolation (named $\mu_0 x$);
3. atomic absorption modelling (named $\mu_1 x$).

After these steps it is possible to obtain the EXAFS signal as

$$\chi(E) = \frac{\mu x(E) - \mu_1 x(E)}{\mu_1 x(E) - \mu_0 x(E)}.$$

Lengerer and Eisenberger [12] suggested a method that is widely used. Atomic absorption modelling is carried out using polynomial curves or cubic splines and is evaluated using Heitler's formula [13]. The edge-jump, which is the only unknown parameter, is calculated with a pre-edge extrapolation.

Fig. 4–6 show the complete signal extraction procedure for metallic Rh.

The raw EXAFS signal obtained with the above procedure is built of many sinusoidal waves. Fourier transform (FT) is the standard tool used for frequency separation. This operation transforms each sinusoidal component in an FT modulus peak, going from k (Å^{-1}) space to R (Å) space. The outcoming function is a radial distribution.

Two problems related to FT exist. First, at high k values, $\chi(k)$ is remarkably damped, therefore little information is contained at those values. To minimise this problem, $\chi(k)$ is multiplied by k_n before Fourier transformation; usually n is equal to 1, 2 or 3. Second, the signal has a limited number of points, therefore Fourier integral is truncated. To minimise distortions and to avoid the presence of ripples in the FT modulus, $\chi(k)$ is multiplied by a window $W(k)$.

The height of FT peaks depends on the amplitude parameters of the EXAFS equation, while their position depends on phase parameters. Total or partial overlapping of more peaks often occurs.

If phase function did not depend on k, maxima of FT peaks would fall at the correct interatomic distances. Since $\Phi(k)$ depends on k (always with a negative slope), peaks are shifted to lower R values [10].

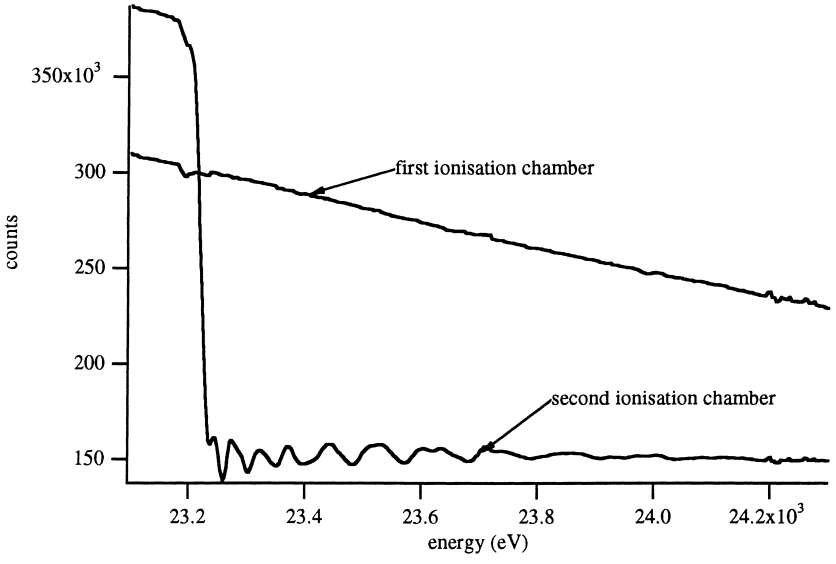

Fig. 4. Raw data for metallic Rh.

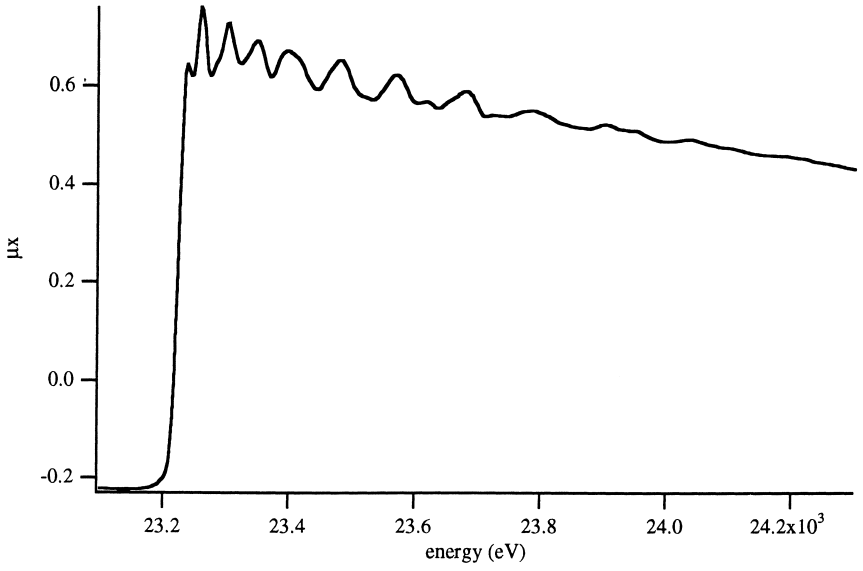

Fig. 5. Absorption spectrum of metallic Rh.

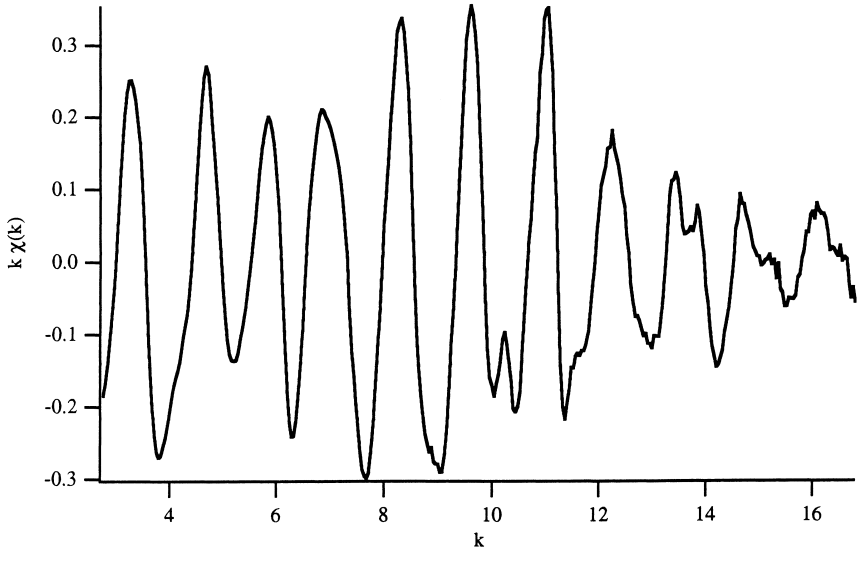

Fig. 6. EXAFS signal of metallic Rh.

Fig. 7 shows the FT modulus for metallic Rh. Peaks corresponding to different Rh–Rh distances are clearly visible.

Once different R values have been separated, an inverse FT is carried out, going from R (Å) space to k ($Å^{-1}$) space, but only on limited intervals in R space. Each peak is individually transformed and the outcome of this operation is a $\chi_i(k)$ function related to absorber–scatterer pairs whose interatomic distances belong to that specific integration interval. Fig. 8 shows the inverse FT (FT^{-1}) of the first peak in Fig. 7, which corresponds to the first Rh–Rh atoms pair.

Structural parameters can be obtained from $\chi_i(k)$ by means of a fitting procedure using known phase

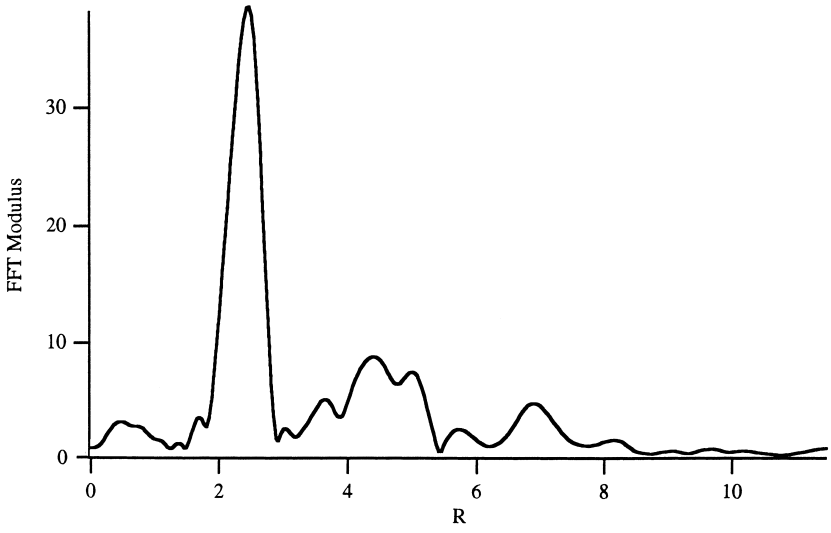

Fig. 7. Fourier transform.

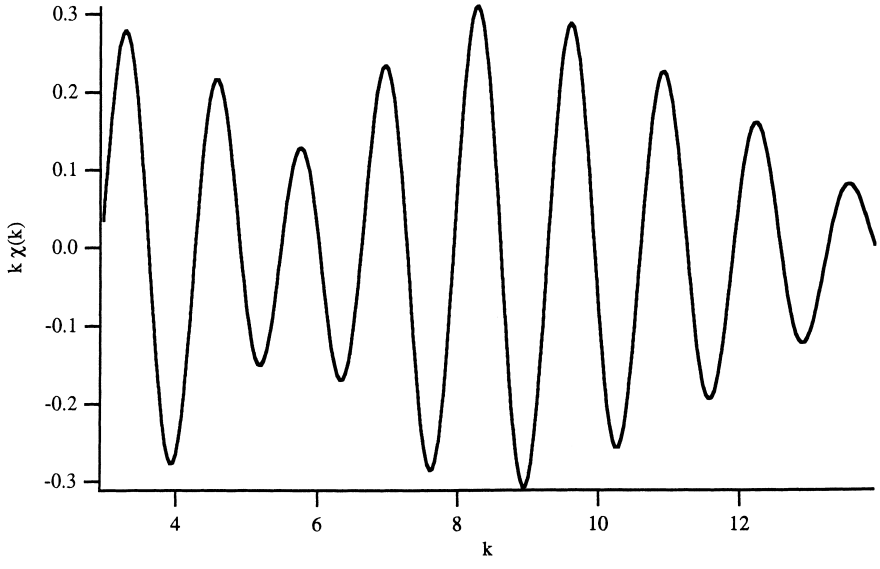

Fig. 8. First peak inverse transform.

and amplitude functions. EXAFS analysis allows to obtain coordination numbers, interatomic distances and an estimate of disorder around the central atom.

Phase and scattering amplitude functions are either theoretical or experimental functions.

Teo et al. [14,15] calculated theoretical functions assuming that the photoelectron wave is plane. Better phases and amplitudes were obtained by McKale et al. [16], within the curved wave approximation; more recently, better theoretical functions were provided by the program FEFF [17].

Experimental functions are extracted from proper reference samples whose structure is already known. These can be used, thanks to the phase and amplitude transferability principle [18] that states as follows:

Phases and amplitudes are insensitive enough to chemical environment in order to be extracted from a well-known sample and transferred to an unknown sample containing the same absorber–scatterer pair at a similar distance.

Phases and amplitudes can be extracted filtering FT peaks one by one and using the following formulas:

$$\Phi(k) = \text{arctg}\frac{\text{Re}}{\text{Im}} - 2kR \quad A(k) = \exp(-2\sigma^2 k_2) \times \exp\left(\frac{-2R}{\lambda(k)}\right) \quad |f(k)| = \sqrt{\text{Re}^2 + \text{Im}^2}\,\frac{R^2}{N}.$$

Experimental amplitude functions include the analyser's estimate of σ and $\lambda(k)$ for the reference sample, so final fitting values for these parameters will be relative to the initial choice.

The k scale is not an absolute one because it depends on the choice of E_0 that is entrusted, in many cases to the analyser's skills. Besides, threshold energy is slightly sensitive to chemical environment and sometimes monochromator fails too, adding other errors. Therefore it is necessary to redefine k scale introducing a ΔE_0 dependence:

$$k' = \sqrt{K^2 + 0.2624\Delta E_0}.$$

This operation aims at bringing phase and amplitude to the same scale of the signal. This is true also using theoretical functions. Even though they are built on an absolute scale it is better to bring them to the experimental one.

Experimental phase and amplitude functions are better than theoretical ones because they do not contain calculus approximations. Anyway analysers must be careful to extract them using the same procedure as with the unknown sample (same integration limits and same windows) in order to introduce exactly the same truncation distortions.

Experimental functions are not always available because no proper reference compounds exist or because it is impossible to extract them. For instance metallic Fe does not allow to extract phase and amplitude for Fe–Fe pair because Fe is surrounded by 8 atoms at 2.48 and 6 atoms at 2.86 Å and these two peaks overlap in the FT modulus.

In these cases the analyser is compelled to use theoretical functions. In order to obtain coordination numbers N_i it is necessary to estimate $\lambda(k)$. One of the used functions, proposed by Lee and Beni [19], is:

$$\lambda(k) = \frac{1}{\Gamma}\left[\left(\frac{\eta}{k}\right)^4 + k\right],$$

where Γ and η are numerical coefficients. η is equal to zero unless minimisation has to be carried over regions with $k<3$. Γ has to be determined by fitting and using a known model.

This technique allows to estimate structural parameters with precision highly dependent on data and analysis quality. Usually errors are of about 0.01–0.02 Å for interatomic distances, and 5–15% for coordination numbers.

5. Data analysis statistics

As in any other technique, outcoming values must have their error bars; particularly in EXAFS, where the analysis is based on fitting procedures, the statistical analysis becomes a very important tool.

The minimisation procedure is carried out over the following function:

$$F(P_i) = A = \sum_k w(k)[\chi_{\text{exp}}(k) - \chi_{\text{th}}(k, P_i)]^2,$$

where P_i are the fitting parameters and $w(k)$ is a weighing function.

A residual factor also can be defined as

$$\rho = \frac{A}{\sum_k w(k)\chi^2_{\text{exp}}(k)}.$$

Another important quantity is the number of independent points N_{ind}, which is strictly related to the maximum number of parameters that can be fitted, given by $N_{\text{par}}=N_{\text{ind}}-1$.

Since the EXAFS signal undergoes two Fourier integrations, the number of independent points is given by the following formula [20]:

$$N_{\text{ind}} = \frac{2 \cdot \Delta k \Delta R}{\pi} + 2,$$

where Δk is the fitting interval (*not* the Fourier integration interval) and ΔR is the filtering interval. The term ''+2'' is due to the discrete nature of data.

The number of degrees of freedom is ν given by: $\nu = N_{ind} - N_{par}$.

Systematic errors in EXAFS measurements can arise from any element in the beam-line. Particularly, the presence of harmonics and inhomogeneities in the sample may reduce signal amplitude and hence lead to deceiving neighbour numbers. Detectors are also error sources, for instance, if detectors are ionisation chambers, the chosen gas is an important factor. An uncontrollable error can derive from the beam itself.

Nowadays there are no standard methods for error determination in EXAFS spectroscopy from experimental errors yet. The following treatment is the one used by our team. It takes care of the recommendations of the Standardisation Committee [8,9], using methods which yield (probably) overestimated errors.

All statistical concepts are based on repeating each single measure three times or more, in order to define an average with its standard deviation. Hence recording each spectrum n times, that is, recording every point n times, the average is given by

$$\overline{k_i\chi(k_i)} = \sum_{j=1}^{n} k_i\chi_j(k_i)/n$$

and standard deviation by

$$s(k_i) = \sqrt{\frac{\sum_{j=1}^{n}\left[\overline{k_i\chi(k_i)} - k_i\chi_j(k_i)\right]^2}{n-1}}.$$

For fitting procedures it is necessary to define a function strictly related to the ''goodness of fit'', hence a function which ''says'' how far the fitting curve is from the experimental data. One of the most used ones is Chi-squared:

$$X_2 = \sum_i \frac{1}{s_i^2}[y_i - y(x_i)]^2,$$

where y_i are experimental data and $y(x)$ is the chosen function. In EXAFS particular case it becomes

$$X^2 = \sum_i \left[\frac{k_i\chi_{exp}(k_i) - k_i\chi_{th}(k_i)}{s^2(k_i)}\right]^2.$$

Another useful quantity is the Reduced Chi-squared defined as follows:

$$X_\nu^2 = \frac{X^2}{\nu}.$$

For a good fit it tends to one. Fits with X_ν^2 lower than one are equally significant as that of those with $X_\nu^2 = 1$.

Once chi-squared has come to a minimum, error determination becomes possible varying each parameter separately while refining the others until X^2 changes of n units, accordingly to the chosen confidence interval. In the case of a confidence interval of 68%, $n=1$. Other values of n are tabulated in proper handbooks.

When a fit has reached a minimum using a certain structural model, a new fit can be performed adding more parameters. A question arises: Does the improvement in fit quality justify a higher number of parameters?

As more parameters are added, fitting function complexity increases while X^2 decreases. However, X_ν^2 behaviour depends on the number of degrees of freedom, which decreases while increasing the number of parameters. One of the most used comparison criteria between two fits is the F-Test [21,22]. It gives a hint on choosing the best fit by comparing their X_ν^2 ratio to those tabulated on Fisher's tables.

More information on statistics can be found on the books written by Taylor [23] and Bevington and Robinson [24].

6. Pt/KL zeolite catalyst under oxidation, reduction and reaction cycles

This work was performed by Bellatreccia et al. [25] and Dossi et al. [26].

This Pt/KL zeolite is a reforming catalyst, very active and selective in conversion of methylcyclopentane (MCP) to benzene. It was prepared via CVD (chemical vapour deposition) at 70°C using platinum hexafluoroacetylacetonate under flowing argon. The amount of Pt deposited was about 1% in weight.

Exploiting EXAFS capability of in situ analysis, spectra were recorded after the following steps:

(A): (1) After deposition; (2) after reduction under H_2; (3) after calcination under O^2; (4) after second reduction under H_2.

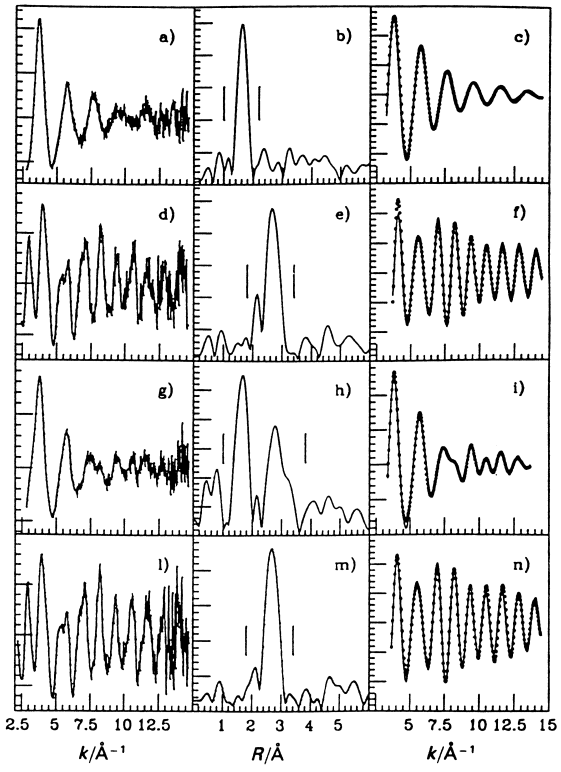

Fig. 9. Analysis results for treatment A.

(B): (1) After reduction; (2) after catalytic test with MCP.

(A) Fig. 9 (a)–(c) show the EXAFS signal, FFT and the first peak filter, respectively, of the sample after deposition. Data analysis shows that there is no Pt–Pt interaction and that the precursor structure is maintained. This stands for a low interaction between the zeolite cage and $Pt–O_4$ groups.

Fit results

Fig. 9	Shell	N	R (Å)	σ^2 (10^{-2} Å)
(c)	Pt–O	4.0±0.4	1.98±0.02	5.6±0.5
(f)	Pt–Pt	5.5±0.5	2.76±0.02	7.3±0.7
(i)	Pt–O	2.5±0.2	2.02±0.02	7.3±0.7
	Pt–Pt	1.0±0.2	2.76±0.02	6.4±0.6
	Pt–Pt	1.0±0.2	3.07±0.02	7.1±0.7
(n)	Pt–Pt	6.0±0.5	2.76±0.02	7.4±0.7

Fig. 9(d)–(f) refers to the sample after first reduction. During this step reduction eliminates ligands and leads to the formation of metal particles. This procedure avoids the initial calcination which leads to the formation of Pt oxide particles. Assuming a close-packed structure, the estimate diameter of the cluster does not exceed 7 Å. The cluster is well confined in the zeolite cavity whose dimensions are 5 Å×13 Å×11 Å, no Pt–O interaction can be seen at this stage. This could have two explanations:

- Pt–O interaction is negligible compared to Pt–Pt interactions and/or
- Pt–O coordination distances cover a wide range, producing a flat distribution on the FFT of the experimental spectrum.

The large amount of noise contained in data prevents from extracting the cluster form [27].

Fig. 9(g), (h) and (l) refers to the sample after calcination. Data analysis reveals the presence of metal particles not completely oxidised to PtO_2, located inside the zeolite cavities.

Fig. 9(1)–(n) refers to the sample after the second reduction. The fit results closely match those obtained after the first reduction. This suggests that the cluster structure remains unchanged after thermal and chemical treatments and no sintering takes place. This conclusion was also confirmed by the fact that its catalytic performances were retained even after two oxidation cycles (not shown here).

(B) Fig. 10(d)–(f) refers to the sample after reduction. They show the same structure of the reduced sample described above.

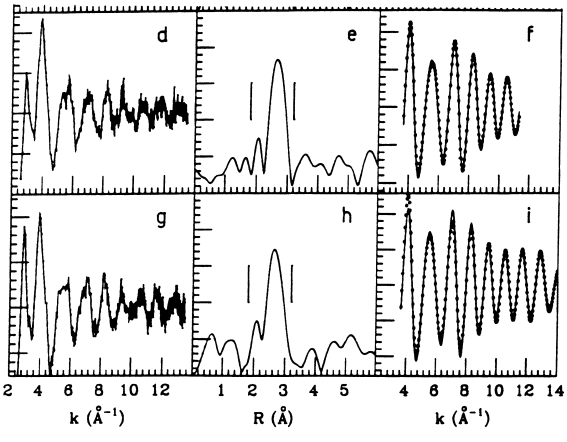

Fig. 10. Analysis results for treatment B.

Fit results

Fig. 10	Shell	N	R (Å)	σ^2 (10^{-2} Å)
(f)	See reduced samples in Fig. 9			
(i)	Pt–Pt	6.1±0.5	2.76±0.02	7.5±0.7

Fig. 10(g)–(i) refers to the sample after a catalytic test with MCP. Data analysis shows no evidence of a Pt–C contribution to the signal. This confirms the absence of a significant carbon deposition on the metal surface. The reactivity of the system remains unchanged after a 24 h work. If it had been coked, the catalyst would have been deactivated.

7. NO decomposition and CO oxidation catalysts (three-way catalysts)

A very efficient catalytic system for NO decomposition and CO oxidation is built by using a solid solution of two oxides as support for noble metals. This solution contains specifically CeO_2 and ZrO_2, while the noble metal is Rh, Pt or Pd.

Pure ZrO_2 is monoclinic. Zr has seven oxygen neighbours at seven different distances [28]. Pure ceria has a fluorite structure. Ce has eight oxygen neighbours at 2.34 Å. When a second oxide like CeO_2 is added to ZrO_2 the structure becomes tetragonal or cubic [29]. Nevertheless, in powder diffraction spectra there are some peaks which cannot belong to these structures.

There are three hypothetical structures for cubic-stabilised zirconia: (1) Eight oxygen atoms at 2.20 Å; (2) four oxygen atoms at 2.07 Å and four at 2.35 Å; (3) six oxygen atoms at 2.14 Å and two at 2.42 Å.

Spectra of the following samples were studied [30,31]: Rh (5% in weight) on: (a) Zr 80% Ce 20% (T); (b) Zr 40% Ce 60% (C); (c) Zr 20% Ce 80% (C); (d) Zr 50% Ce 50% (C); (e) Zr 50% Ce 50% (T). Here T stands for tetragonal, C for cubic and the percentages are molar ratios. Each spectrum was recorded at Zr and Rh K edges, and at L_{III} Ce edge as prepared, after reduction and after catalytic cycles with NO, CO and NO+CO.

The following discussion aims at determining whether the two oxides form a solid solution or stay separated and, if the first hypothesis were confirmed, at solving the sample structure.

Fig. 11 shows how FFT modulus changes as molar ratio changes. The second peak remarkably varies in height from one sample to another. The decreasing magnitude of the Zr-cation peak has always been explained as owing to an increasing static disorder [32]. Actually peak heights decrease because Zr–Zr and Zr–Ce phases oppose each other, that is, there is a

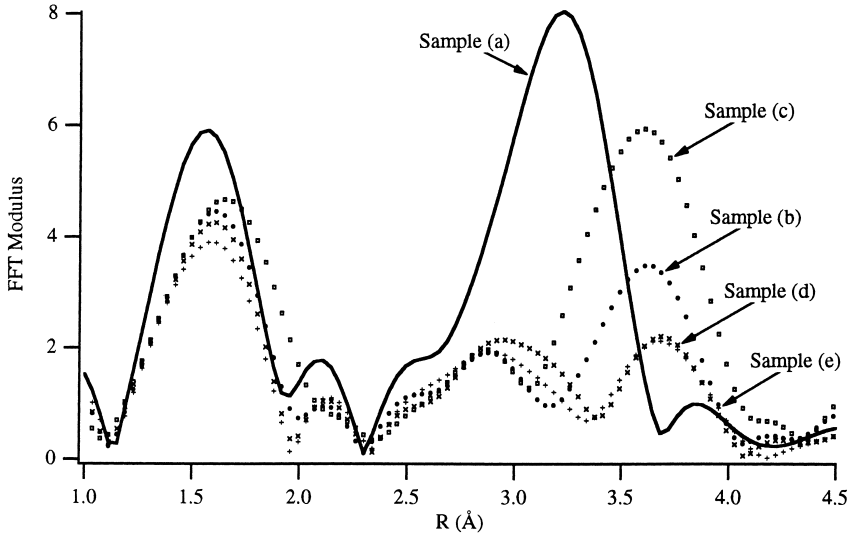

Fig. 11. FFT modula of the investigated samples.

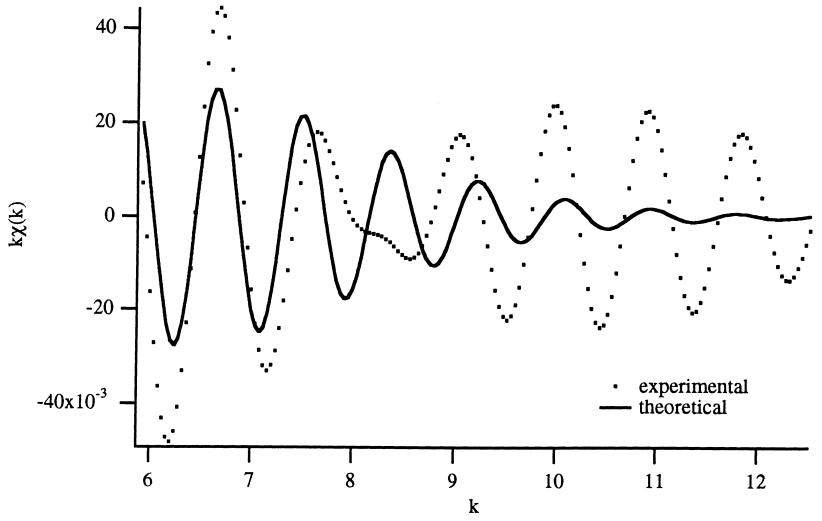

Fig. 12. Fit of the II shell with 12 Zr.

difference of n between the two functions (that means that the EXAFS signals of Zr–Zr and Zr–Ce pairs are almost opposite to each other).

The question on whether the oxides form a solid solution or stay basically separated constituting microphases is still open. Fig. 12 and 13 show two fits carried out (for R between 2.3 and 4.1 Å on sample (d) for k>6 $Å^{-1}$, in order to make negligible the presence of oxygen atoms. The first one was performed assuming that the oxides stay separated, hence considering each Zr surrounded by 12 Zr neighbours. The second one simulates a solid solution in which each Zr is surrounded by a total amount of 12 Zr and Ce neighbours with coordination numbers according to their molar ratios. The hypothesis of a solid solution is obviously confirmed, Fig. 14 shows the fit carried out over the entire k-space interval, including oxygen atoms in the theoretical spectrum. Numerical results are reported in Table 1.

Fitting the first peak filter was a hard task. None of the structures suggested in literature for cubic-stabilised zirconia worked out as expected (for an example

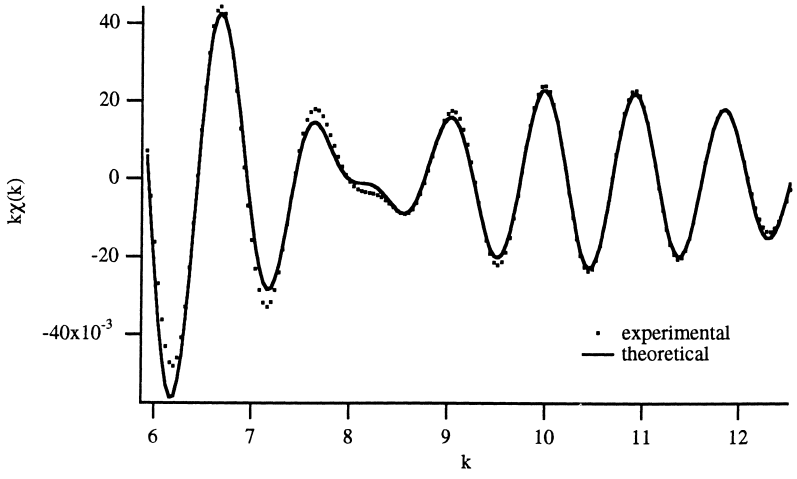

Fig. 13. Fit of the II shell with 12 Zr and Ce.

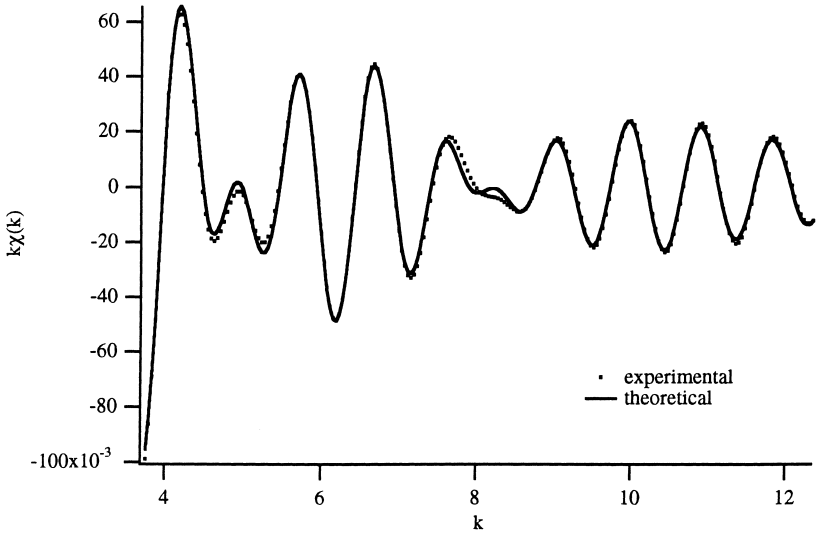

Fig. 14. Fit carried out over the whole EXAFS signal with 12 Zr and Ce.

Table 1
Local coordination models for sample (d), fitted to EXAFS signal at Zr K edge

		Coordination no.	R (Å)	σ (Å)	ΔE (eV)	X_ν^2
II shell (Fig. 14)	Zr–Zr	6	3.64±0.04	0.105±0.006	−10±4	0.94
	Zr–Ce	6	3.72±0.01	0.095±0.006	−7±2	
	Zr–O	24	4.24±0.04	0.139±0.010	−8±2	
I shell (Fig. 15)	Zr–O	8	2.113±0.007	0.142±0.010	−3.4±6	21.2
I shell (Fig. 16)	Zr–O	4	2.115±0.008	0.078±0.008	0.0±0.5	1.9
	Zr–O	2	2.324±0.011	0.078±0.008	0.0±0.5	

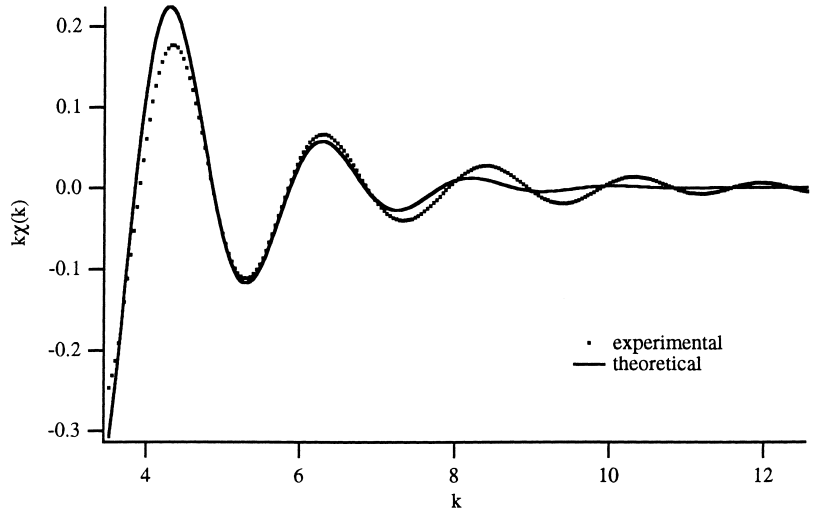

Fig. 15. Fit of I shell with 8 O at same distance.

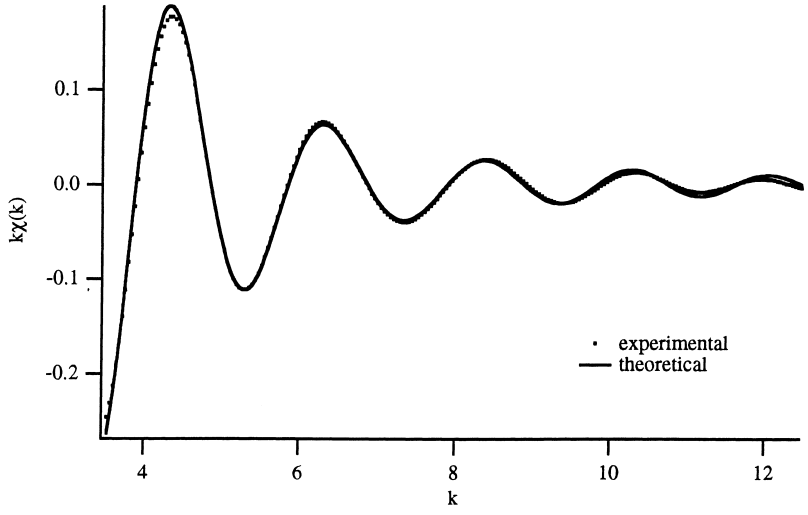

Fig. 16. Best fit of I shell.

see Fig. 15, where the fit was performed on the basis of a single Zr–O distance model), so various sets of coordination numbers and distances were tested (more than 40 Å). Theoretical functions containing from one to three different interatomic distances and total coordination numbers between six and eight atoms were examined. At the end more than a single reasonable fit was obtained, therefore only a statistical analysis, carried out with the F test, allowed to settle which one was the best (Fig. 16). Numerical results are listed in Table 1.

The fit that survived this statistical comb can be explained keeping in mind the ideal fluorite structure. Fit results suggest that two oxygen atoms around each Zr go further away and approach another atom while keeping Ce–O distances unchanged. This hypothesis is also confirmed by data analysis of spectra taken at Ce edge, and by Raman spectroscopy.

References

[1] H. Bertagnolli, T.S. Ertel, Angew. Chem. Int. Ed. Engl. 33 (1994) 45.
[2] W.H. McMaster, N.K. del Grande, J.H. Mallet, J.H. Hubbel, Compilation of X-ray cross sections, UCPL-50174 sec. II rev. 1 (1969).
[3] B.K. Teo, EXAFS: Basic Principles and Data Analysis, Springer, Berlin, 1986.
[4] E.A. Stern, Phys. Rev. B 10 (1974) 3027.
[5] P.A. Lee, P.H. Citrin, P. Eisenberger, B.M. Kincaid, Rev. Mod. Phys. 53 (1981) 769.
[6] R. Frahm, Nucl. Instrum. Meth. Phys. Res. A270 (1988) 578.
[7] E. Dartyge, C. Depautex, J.M. Dubuisson, A. Fontaine, A. Jucha, P. Leboucher, G. Tourillon, Nucl. Instrum. Methods A 246 (1986) 452.
[8] Report of the International Workshop on Standards and Criteria in X-Ray Absorption Spectroscopy, Physica B 158 (1989) 701.
[9] Report of the International Workshop on Standards and Criteria in X-Ray Absorption Spectroscopy, in: S.S. Hasnain (Ed.), X-Ray Absorption Fine Structure, Hellis Horwood, Chicester, 1991.
[10] A. Michalowlcz, in: Societé Française de Chimie (Ed.), Logiciels pour la Chimie, Paris, 1991.
[11] A. di Cicco, Physica B 208–209 (1995) 125.
[12] B. Lengerer, P. Eisenberger, Phys. Rev. B 21 (1980) 4507.
[13] W. Heitler, in: Quantum Theory of Radiation, 3rd ed., Oxford University Press, Oxford.
[14] B.K. Teo, A.P. Lee, A.L. Simmons, P. Eisenberger, B.M. Kincaid, J. Am. Chem. Soc. 99 (1977) 3854.
[15] P.A. Lee, B.K. Teo, A.L. Simmons, J. Am. Chem. Soc. 99 (1977) 3856.
[16] A.G. McKale, B.W. Veal, A.P. Paulikas, S.K. Chan, G.S. Knapp, J. Am. Chem. Soc. 110 (1988) 3763.
[17] J.J. Rehr, I.M. de Leon, S.I. Zabinsky, R.C. Albers, J. Am. Chem. Soc. 113 (1991) 3763.
[18] P.H. Citrin, P. Eisenberger, B.M. Kincald, Phys. Rev. Lett. 36 (1976) 1346.
[19] P.A. Lee, G. Beni, Phys. Rev. B 15 (1977) 2862.
[20] E.A. Stern, Phys. Rev. B 48 (1993) 9825.
[21] R.W. Joyner, K.J. Martin, P. Meehan, J. Phys. C 20 (1987) 4005.

[22] J. Freund, Phys. Lett. A 157 (1991) 256.
[23] J.R. Taylor, An Introduction to Error Analysis, Oxford University Press, Oxford, 1982.
[24] P.R. Bevington, D.K. Robinson, Data Reduction and Error Analysis for the Physical Sciences, McGraw-Hill, New York, 1992.
[25] M. Bellatreccia et al., J. Chem. Soc. Faraday Trans. 91 (1995) 2045.
[26] C. Dossi et al., J. Catal. 145 (1994) 377.
[27] P. Lagarde, T. Murata, G. Vlalc, H. Dexpert, E. Freund, J.P. Bournonville, J. Catal. 84 (1983) 333.
[28] D.K. Smith, H.W. Newkirk, Acta Crystallogr. 18 (1965) 983.
[29] C.J. Howard, R.J. Hill, B.E. Reichert, Acta Crystallogr. B44 (1988) 116.
[30] G. Ranga Rao, P. Fornasiero, R. di Monte, J. Kaspar, G. Vlaic, G. Balducci, S. Meriani, G. Gubitosa, A. Cremona, M. Graziani, J. Catal. 162 (1996) 1.
[31] G. Vlaic, P. Fornasiero, S. Geremia, J. Kaspar, M. Graziani, J. Catal. 168 (1997) 386–392.
[32] P. Li, I.W. Chen, J.E. Penner-Hahn, J. Am. Ceram. Soc. 77 (1994) 1281.